CEST 2023

18th International Conference on Environmental Science and Technology

Athens, Greece, 30 August to 2 September 2023

Short-time numerical simulation of ultrasonically assisted electrochemical removal of strontium from water

LICHT K.[1*], LONČAR G.[1], POSAVČIĆ H.[1], HALKIJEVIĆ I.[1]

[1] Department of Hydroscience and Engineering, Faculty of Civil Engineering, University of Zagreb, Andrije Kačića-Miošića 26, 10000 Zagreb, Croatia

*corresponding author:
e-mail:katarina.licht@grad.unizg.hr

Abstract 3D numerical simulations and measurements on an electrochemical reactor were used to analyze the efficiency of strontium removal from water, with and without simultaneous ultrasound treatment. Ultrasound was generated using 4 ultrasonic transducers with an operating frequency of 25 kHz. The reactor used 8 aluminum electrodes arranged in two blocks. Strontium ions in water are modeled as particles characterized by a charge of $3.2 \cdot 10^{-19}$ C and a diameter of $1.2 \cdot 10^{-8}$ m. The numerical model was created in Flow-3D software using the basic hydrodynamic module, electrostatic module, and general moving objects module. The performance of the studied reactor variants by numerical simulations is defined by the ratio of the number of model strontium particles permanently retained on the electrodes at the end of the simulation period to the initial number of particles in the water. For the laboratory reactor, the effect of strontium removal is defined by the ratio of the homogeneous strontium concentration in the water at the end and at the beginning of the experiments.
The results show that the use of ultrasound increases the effect of strontium removal from 10.3% to 11.2% after 180 seconds of water treatment. The results of numerical simulations agree with the results of measurements on a reactor with the same geometrical characteristics.
Keywords: numerical model, electrochemical reactor, strontium

1. Introduction

Strontium (Sr) is a naturally occurring element found in many sedimentary rocks and some calcite minerals. Significant anthropogenic sources include industrial activities, fertilizers, and nuclear fallout (Scott et al., 2020). Sr concentrations greater than 1.5 mg L^{-1} in water can cause strontium rickets and other health problems in humans, especially in children (Epa et al., n.d.; Peng et al., 2021; Scott et al., 2020). Elevated Sr concentrations have been reported in drinking water worldwide, with concentrations as high as 52 mg L^{-1} in groundwater in the northern USA (Luczaj and Masarik, 2015; Peng et al., 2021; Scott et al., 2020). One of the possible remediation technologies for Sr is an electrochemical process (Kamaraj and Vasudevan, 2015). These processes are based on in-situ coagulant formation through the application of electric current to metal electrodes. The process consists of dissolution of the sacrificial anode, formation of hydroxide ions and hydrogen at the cathode, electrolyte reactions at the electrode surface, adsorption of coagulants on colloidal impurities and electrodes, and removal of the resulting flocs by precipitation or flotation (Mollah et al., 2001). One of the main drawbacks of the process is the polarization and passivation of the electrodes, which can be minimized by combining it with ultrasonication (Dong et al., 2016; Ince, 2018; Moradi et al., 2021). Ultrasonic cavitation can result in solute thermolysis and the formation of reactive species such as hydroxyl radicals and hydrogen peroxide (Mohapatra and Kirpalani, 2019). It also increases the mass transfer rates of solutes and enhances the surface properties of solid particles (Fu et al., 2016; Ziylan et al., 2013).

The aim of this research is to evaluate the efficiency of the electrochemical (EC) batch reactor with and without the additional use of ultrasound (US), which is intended for the purification of water mainly contaminated with an increased concentration of Sr. The results of the 3D numerical simulations are verified by measurements in the laboratory EC reactor.

2. Methodology

2.1. Laboratory EC reactor and measurements

The experimental setup, Figure 1, consisted of a modified US bath with 4 transducers at the bottom and a total of 200 W of nominal ultrasonic power (TI-H 10 MF2 from Elma Ultrasonics, Germany). An operating frequency of 25 kHz was used. The bath was divided into two sections by a baffle to ensure even flow between electrodes. Each section housed a specially designed electrode stand that held 4 electrodes – 2 cathodes and two anodes. Electrodes were connected to the 3000 W power supply (CSP-3000-120 from Mean Well, Taiwan), controlled by the output voltage of the function generator (JT-JDS6600 from Joy It, Germany). The electrodes, with an active anode surface area of 182.64 cm^2 (1 anode), were arranged as shown in Figure 2, with an interelectrode distance of 1 cm. A voltage of 60 V was used in all experiments. 5.5 L of Sr solution was treated for 180 s.

The measurement of the strontium concentration was carried out at 3 uniformly distributed points across the horizontal section, at the depth of the middle of the electrodes. Strontium concentrations were measured on

an Agilent 5900 SVDV ICP-OES system with an instrumental detection limit of 0.01 µg L^{-1} in radial viewing mode. The analysis was carried out in accordance with the EPA 200.7 method. The relative standard deviation (% RSD) for repeated measurements of the same samples was an average of 0.4.The mean value of the initial strontium concentrations measured at the three measurement points was 3 mg L^{-1}.

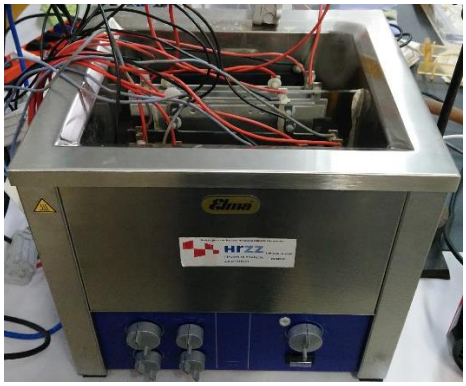

Figure 1. US bath modified as an EC reactor

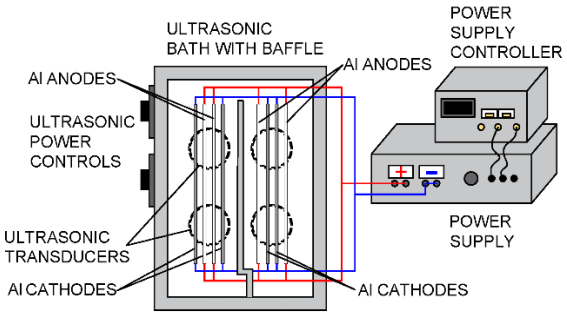

Figure 2. Schematic view of the experimental set-up

2.2. Modeled EC reactor

Metal electrodes immersed in water produce an electrostatic field whose intensity depends primarily on the potential difference between the anode (A) and the cathode (K) and the distance between the electrodes. In the solution, Sr is present in ionized form (Sr^{2+}), so when an electrostatic field is applied, the Sr ions move toward the cathode and accumulate there (electrodeposition). The efficiency of Sr removal depends on the configuration of the electrode plates and the applied voltage. A voltage of 60 V was used in all the analyzes.

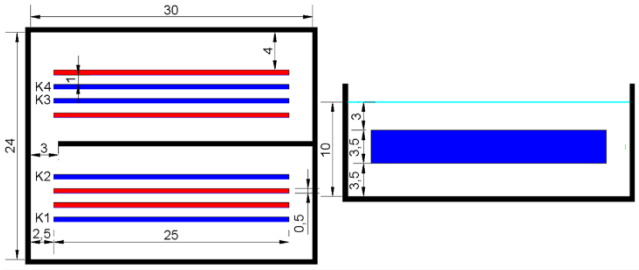

Figure 3. Schematic view of a modeled EC reactor with basic dimensions in cm (K-cathode, A-anode)

The adopted spatial domain of the reactor is defined by a length of 0.3 m and a width of 0.24 m (Figure 3). The electrode plates are made of aluminum, have a length of 0.25 m, a height of 0.035 m, and a thickness of 0.005 m, and are raised from the bottom to a height of 0.035 m. The water depth is constant at 0.1 m. The electrodes are arranged in two blocks of 4 electrodes each, K-A-A-K for the lower block and A-K-K-A for the upper block. The distance between the electrodes is 0.01 m. The numerical simulations were performed for a period of 180 s.

2.3. Numerical model

The numerical model was created in Flow-3D software using the basic hydrodynamic module, electrostatic module, and general moving objects (GMO) module. A structured mesh in the Cartesian coordinate system is used, and the boundary conditions are defined on 6 flat surfaces with the block discretization method. The so-called volume of fluid (VOF) formulation is used to incorporate impermeable boundaries in the mesh and the corresponding system of equations. 3D impermeable objects are treated as a set of finite volumes with associated surfaces, which supports the possibility of solving systems of differential equations on orthogonal and structured grids. The calculation of the free surface is carried out using the VOF technique based on the volume fraction of each computational 3D cell.

The mass conservation equation (continuity equation, 1) and the momentum conservation equation (Navier-Stokes equation, 2-4) in the Cartesian coordinate system are described as:

$$V_f \frac{\partial \rho}{\partial t} + \frac{\partial}{\partial x}(\rho u A_x) + \frac{\partial}{\partial y}(\rho v A_y) + \frac{\partial}{\partial z}(\rho w A_z) = R_{DIF} + R_{SOR} \quad (1)$$

$$\frac{\partial u}{\partial t} + \frac{1}{V_f}\left(u A_x \frac{\partial u}{\partial x} + v A_y \frac{\partial v}{\partial y} + w A_z \frac{\partial w}{\partial z}\right) = -\frac{1}{\rho}\frac{\partial p}{\partial x} + f_x \quad (2)$$

$$\frac{\partial v}{\partial t} + \frac{1}{V_f}\left(u A_x \frac{\partial u}{\partial x} + v A_y \frac{\partial v}{\partial y} + w A_z \frac{\partial w}{\partial z}\right) = -\frac{1}{\rho}\frac{\partial p}{\partial y} + f_y \quad (3)$$

$$\frac{\partial w}{\partial t} + \frac{1}{V_f}\left(u A_x \frac{\partial u}{\partial x} + v A_y \frac{\partial v}{\partial y} + w A_z \frac{\partial w}{\partial z}\right) = -\frac{1}{\rho}\frac{\partial p}{\partial z} + G_z + f_z \quad (4)$$

where: *u, v, z* are the components of the velocity vector in the x, y, z directions; R_{DIF} turbulent diffusion term; *p* pressure; R_{SOR} source or sink member; *Ax, Ay, Az* flow cross sections in calculation cell; *ρ* liquid density (1000 kg m^{-3}); *Gz* gravitational acceleration; *fx, fy, fz* acceleration due to viscous action in the x, y, z directions based on the divergence of the viscous stress tensor σ ((1/ρ)∇.σ); *Vf* volume fraction of the liquid (fluid) in the calculation cell calculated based on equation 5, in which *F* is the volume fraction with values from 0 to 1. A *F* value of 0 indicates that the cell is completely filled with gas, and a value of 1 indicates it is completely filled with liquid.

$$\frac{\partial F}{\partial t} + \frac{1}{V_f}\left[\frac{\partial (F A_x u)}{\partial x} + \frac{\partial (F A_y v)}{\partial y} + \frac{\partial (F A_z w)}{\partial z}\right] = 0 \quad (5)$$

The solutions of the Laplace equation for the spatial distribution of the electric potential (6) and the electric field strength (7) are also found using the numerical model, which enables the further solution of the dynamic equation (8) for the motion of particles under the action of an electrostatic field.

$$\nabla \cdot (K \nabla \phi) = 0 \quad (5)$$

$$E = -\nabla\phi \quad (6)$$

$$\frac{d\boldsymbol{u}_P}{dt} = g - \frac{1}{\rho_P}\nabla p + \alpha(\boldsymbol{u} - \boldsymbol{u}_P) + \beta(\boldsymbol{u} - \boldsymbol{u}_P)|\boldsymbol{u} - \boldsymbol{u}_P|\frac{\rho}{\rho_P} + e_i E \quad (7)$$

ϕ is the electric potential (0 V at the cathode and 60 V at the anode); E electric field strength, K dielectric constant of the material (for water = 80.5, aluminum electrodes = 5, insulating polymer material on the reactor walls = 5); $\boldsymbol{u}_P$ particle velocity vector; ρ_P particle density (1000 kg m^{-3}); $\boldsymbol{u}$ the velocity vector of the liquid (water), α and β shape resistance coefficients for particles of diameter dp ($\alpha = 0$, $\beta = 0.05$, $dp = 1.2 \cdot 10^{-8}$ m) divided by the mass of the particle; ei is the electric charge of the particle ($3.6 \cdot 10^{-19}$ C) divided by the mass of the particle.

Sr^{2+} ions are modeled as particles with a $3.2*10^{-19}$ C charge and a $1.2*10^{-8}$ m diameter. A total of 4200 particles are initially placed in the water of the model reactor in a grid formation of 30*14*10 in the x, y and z directions.

The spatial domain of the model is discretized by a mesh with cells of equidistant length in the x, y, and z directions of 0.005 m, for a total of 94800 cells.

A laminar flow model and a no-slip wall shear boundary condition are used in performing the simulations. Heat transfer is not considered, due to the short period of time analyzed. The pressure term is solved with an implicit method, while the viscous stresses are solved explicitly.

The boundary conditions of the calculation block (X_{min}, X_{maks}, Y_{min}, Y_{maks}, Z_{min}) are defined as "wall", while at the edge Z_{maks} is given atmospheric pressure with only the gas (air) phase present. A fixed potential is given on the surfaces of the electrodes, while on the edges (reactor walls), the potential is dynamically calculated with the condition $\nabla\phi = 0$. The initial conditions are given as a state of rest of water with a free surface set at 0.1 m, and a hydrostatic pressure distribution.

The contribution of ultrasound is modeled using the GMO module. Four simple supported edge rectangular membranes with an area of 0.02 m x 0.02 m and a thickness of 0.001 m are placed at the bottom of the reactor. The frequency of deformation of the membranes is 25 kHz. and the force amplitude is 0.01 N.

3. Results and discussion

The performance of the investigated reactor configurations through numerical simulations is defined by the ratio of the number of model Sr particles permanently retained on the electrodes at the end of the simulation period to the initial number of particles in the water (30*14*10=4200 particles). Figure 3 shows a comparison of the time series for this ratio for cathodes 1-4. Cathode 2 makes the largest contribution to Sr removal. Furthermore, the contribution of ultrasound to the removal of Sr is more pronounced at cathodes 1 and 4 than at cathodes 2 and 3. The use of ultrasound increases the overall effect of Sr removal from 10.3% to 11.2% after 180 seconds of water treatment. Of the total Sr removed without the effect of ultrasound, 22% accumulated on cathode 1, 31% on cathode 2, 24% on cathode 3, and 23% on cathode 4. Activation of ultrasound changed the effect of removal so that 24% of the total Sr removed accumulated on cathode 1, 31% on cathode 2, 22% on cathode 3, and 25% on cathode 4.

Calculations were also carried out with a reduction in the step of the budget grid from 0.005 m to 0.0025 m, and the deviation of the results (effective) was less than 0.1%. A slightly greater effect with the application of the step of the budget grid of 0.0025 m.

On the laboratory reactor with the same geometry, the effect of Sr removal is defined by the ratio of the final and initial homogeneous concentrations of Sr in water. Measurements on a laboratory reactor were carried out with the aim of verifying numerical simulations. The concentration of Sr is measured by ICP-OES analysis. The results show that after 180 seconds of water treatment, 8.2% of Sr is removed without ultrasound and 9.3% with simultaneous application of ultrasound.

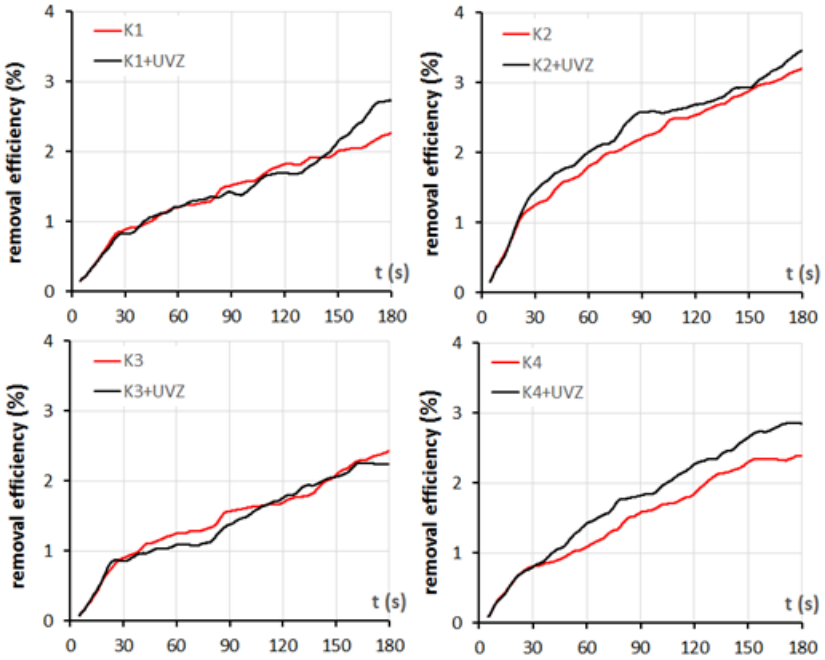

Figure 4. Comparison of the time series for the ratio of model Sr particles accumulated on cathodes 1-4 and particles initially placed in the EC reactor (K1- cathode 1, …, K4- cathode 4).

4. Conclusion

Numerical analyses of the removal of strontium from water by an electrochemical process with and without the simultaneous effect of ultrasound were carried out. It can be concluded that the contribution of ultrasound to the removal of Sr is less than 1%. In the planned continuation of the research, a reactor with the same geometrical and hydraulic characteristics will be analysed in flow-through operation with higher ultrasonic power.

Acknowledgment

This research was funded in part by the Croatian Science Foundation under the project "UIP-2020-02-1160-Purification of Microbiologically and Chemically Contaminated Drinking Water by Electrochemical and Ultrasonic Processes".

References

Dong, B., Fishgold, A., Lee, P., Runge, K., Deymier, P. and Keswani, M. (2016), Sono-electrochemical recovery of metal ions from their aqueous solutions, *Journal of Hazardous Materials*, **318**, 379–387. https://doi.org/10.1016/J.JHAZMAT.2016.07.007

EPA. (2014), Announcement of Final Regulatory Determinations for Contaminants on the Third Drinking Water Contaminant Candidate List. Retrieved from http://fdsys.gpo.gov/fdsys/search/home.action

Fu, F., Lu, J., Cheng, Z. and Tang, B. (2016), Removal of selenite by zero-valent iron combined with ultrasound: Se(IV) concentration changes, Se(VI) generation, and reaction mechanism, *Ultrasonics Sonochemistry*, **29**, 328–336. https://doi.org/10.1016/j.ultsonch.2015.10.007

Ince, N.H. (2018), Ultrasound-assisted advanced oxidation processes for water decontamination, *Ultrasonics Sonochemistry*, **40**, 97–103. https://doi.org/10.1016/j.ultsonch.2017.04.009

Kamaraj, R. and Vasudevan, S. (2015), Evaluation of electrocoagulation process for the removal of strontium and cesium from aqueous solution, *Chemical Engineering Research and Design*, **93**, 522–530. https://doi.org/10.1016/j.cherd.2014.03.021

Luczaj, J. and Masarik, K. (2015), Groundwater Quantity and Quality Issues in a Water-Rich Region: Examples from Wisconsin, USA, *Resources*, **4**(2), 323–357. https://doi.org/10.3390/resources4020323

Mohapatra, D.P. and Kirpalani, D.M. (2019), Selenium in wastewater: fast analysis method development and advanced oxidation treatment applications, *Water Science and Technology: A Journal of the International Association on Water Pollution Research*, **79**(5), 842–849. https://doi.org/10.2166/wst.2019.010

Mollah, M.Y.A., Schennach, R., Parga, J.R. and Cocke, D.L. (2001), Electrocoagulation (EC)- Science and applications, *Journal of Hazardous Materials*, **84**(1), 29–41. https://doi.org/10.1016/S0304-3894(01)00176-5

Moradi, M., Vasseghian, Y., Arabzade, H. and Khaneghah, A.M. (2021), Various wastewaters treatment by sono-electrocoagulation process: A comprehensive review of operational parameters and future outlook, *Chemosphere*, **263**, 128314. https://doi.org/10.1016/J.CHEMOSPHERE.2020.128314

Peng, H., Yao, F., Xiong, S., Wu, Z., Niu, G. and Lu, T. (2021), Strontium in public drinking water and associated public health risks in Chinese cities, *Environmental Science and Pollution Research International*, **28**(18), 23048. https://doi.org/10.1007/S11356-021-12378-Y

Scott, V., Juran, L., Ling, E.J., Benham, B. and Spiller, A. (2020), Assessing strontium and vulnerability to strontium in private drinking water systems in Virginia, *Water*, **12**(4). https://doi.org/10.3390/w12041053

Ziylan, A., Koltypin, Y., Gedanken, A. and Ince, N.H. (2013), More on sonolytic and sonocatalytic decomposition of Diclofenac using zero-valent iron, *Ultrasonics Sonochemistry*, **20**(1), 580–586. https://doi.org/10.1016/j.ultsonch.2012.05.005

PAPER TEMPLATE